ARTICLE

Rhodium(II)/Rhodium(III) Redox Couple for C–H Bond Amination with Alkylazides: a Rhodium(III)-nitrenoid Intermediate with a Tetradentate [14]-Macrocyclic Ligand

Received 00th January 20xx,
Accepted 00th January 20xx

DOI: 10.1039/x0xx00000x

Hideki Sugimoto,*[a] Megumu Sakaida,[a] Yoshihito Shiota,[b] Mayuko Miyanishi,[b] Yuma Morimoto,[a] Kazunari Yoshizawa, *[b] and Shinobu Itoh*[a]

Catalytic activity of a rhodium(II) dimer complex, [Rh^{II}(TMAA)]$_2$, (TMAA = tetramethyltetraaza[14]annulene) in C-H amination reactions with organic azides is explored. Organic azides (N_3-R) with an electron-withdrawing group such as a sulfonyl group (trisylazide; R = S(O)$_2$^{iPr3}C$_6$H$_2$ (Trs)) and a simple alkyl group (R = (CH$_2$)$_4$Ph, (CH$_2$)$_2$OCH$_2$Ph, CH$_2$Ph, C$_6$H$_4$NO$_2$) are employed in intra- and intermolecular C–H bond amination reactions. The spectroscopic analysis using ESI-mass and EPR spectroscopies on the reaction intermediate generated from [Rh^{II}(TMAA)]$_2$ and N_3-R reveals that a rhodium(III)-nitrenoid species is an active-oxidant in the C-H bond amination reaction. DFT calculations suggest that the species can be featured with a radical localised nitrogen atom. The DFT calculation studies also indicate that the amination reaction involves hydrogen atom abstraction from the organic substrate R'–H by the NR moiety of **2$^{N•Trs}$** and successive rebound of the generated organic radical intermediate R'• to [Rh^{III}(NH–R)(TMAA)], giving [Rh^{II}(TMAA)] and R'–NH–R (amination product).

Introduction

Rhodium catalysed C-H bond amination is one of the powerful methods for direct amination of aliphatic and aromatic compounds.[1-11] There are two ways for such reaction. The first one involves formation of an organometallic intermediate with a rhodium–carbon σ-bond generated by oxidative addition of an aliphatic C–H bond to a low valent rhodium center or electrophilic substitution of an aromatic C–H bond by a rhodium species.[6,7,10,11] Coordination of an amine source to the rhodium center and successive reductive elimination give an aminated product. The second one employs a rhodium–nitrenoid (Rh-NR) species, which induces insertion of the NR group into a C-H bond.[1-5,8,9] The latter method is highly promising for C(sp^3)–H amination when a paddle-wheel rhodium(II) dimer, [Rh$_2$(R$_1$COO)$_4$], and an organic azide (N_3-R) or iminoiodinanes (R$_2$I-NR) are used as a catalyst and a nitrene source, respectively (Fig. 1).[1-5,8,9] Involvement of a nitrenoid adduct of a paddle-wheel dirhodium(II) complex in nitrene transfer into C(sp^3)-H bond has also been proposed by calculation studies.[12] Modification of the bridging carboxylate groups of the rhodium(II) dimer complex enabled site-, stereo-, diastereo- and enantio-selective C-H amination reactions. Based on the crystal structure analysis of a nitrene adduct of a paddle-wheel rhodium(II) dimer, [Rh$_2$(esp)$_2$] (esp = α,α,α′,α′-tetramethyl-1,3-benzenedipropanamidate), it has been concluded that the two rhodium centers keep a divalent state with a metal-metal single bond character.[13,14] It has been also revealed that the bond between one rhodium(II) center and the nitrene nitrogen atom has a formally double bond character consisting of the nitrogen→rhodium σ donation and the dirhodium→nitrogen π back donation (1/2π + 1/2π). However, organic azides (N_3-R) used as the nitrene sources have been limited to those having strong electron-withdrawing groups such as sulfinyl (-SO$_2$R") and carboxyl (-CO$_2$R") groups in order to enhance the π back donation by decreasing the energy of the empty N$_p$ orbital.[1-5,8,9] Thus, in C(sp^3)-H amination, it is highly desired to develop a rhodium-nitrenoid active species that can be generated by using non-activated simple organic azides as a nitrene source.

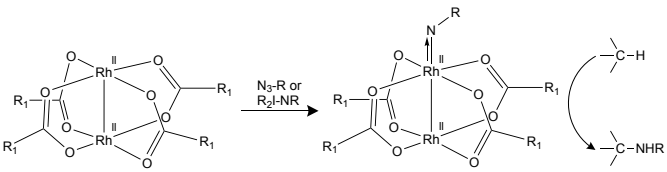

Fig. 1 Nitrene adduct of paddle-wheel dirhodium(II) complex stabilised by π-back donation from dirhodium(II) core to nitrene.

[a] *a/Prog. Dr. H. Sugimoto, M. Sakaida, a/Prof. Dr. Y. Morimoto, Prof. Dr. S. Itoh*
Department of Molecular Chemistry, Division of Applied Chemistry
Graduate School of Engineering, Osaka University
Yamadaoka, Suita, Osaka 565-0871 (Japan)
E-mail:sugimoto@chem.eng.osaka-u.ac.jp, shinobu@chem.eng.osaka-u.ac.jp
[b] *a/Prof. Y. Shiota, M. Miyanishi, Prof. Dr. K. Yoshizawa*
Institute for Materials Chemistry and Engineering and International Research Center for Molecular System, ,
Kyushu University
Motooka, Nishi-ku, Fukuoka, 819-0395 (Japan)
kazunari@ms.ifoc.kyushu-u.ac.jp

† Electronic Supplementary Information (ESI) available: Table S1–S10, Figures S1–S10. Cartesian coordinates. CCDC-2240612 and 2240613 contain the supplementary crystallographic data for this paper. See DOI: 10.1039/x0xx00000x. These data can be obtained free of charge via www.ccdc.cam.ac.uk/data_request/cif, or by emailing data_request@ccdc.cam.ac.uk, or by contacting The Cambridge Crystallographic Data Centre, 12 Union Road, Cambridge CB2 1EZ, UK; fax: +44 122 336033.

To this end, we focus on a rhodium dimer complex, $[Rh^{II}(TMAA)]_2$ (TMAA = tetramethyltetraaza[14]annulene), since it exhibits an interesting structural feature and reactivity.[15] The two rhodium(II) centers are solely connected with a metal–metal single bond, which easily dissociates into two paramagnetic d^7 rhodium(II) monomers, $[Rh^{II}(TMAA)]$ (**1**), in a solution at high temperature (Fig. 2(a)).[15] The rhodium(II) monomer **1** has been demonstrated to work as a strong reductant or a strong nucleophile. For example, the reaction of **1** with carbon monoxide (CO) gives the formyl complex, $[Rh^{III}(CHO)(TMAA)]$, in the presence of dihydrogen (H_2).[16,17] Acetylene (HC≡CH) is reduced by **1** to give the alkene complex, $[Rh^{III}_2(\mu\text{-}C_2H_2^{2-})(TMAA)_2]$.[16,17] Such reactivity of **1** is ascribed to the presence of one unpaired electron in a d_{xz} ($d\pi$) orbital (Rh) supported by the 2,4-pentane-diaminato chelating ligand. Interaction between the unpaired electron on the rhodium(II) center and the electrons in the filled $p\pi$ orbitals of the ligand make energy of the d_{xz} orbital higher. We expect that such a high electron donor ability of **1** enables the Rh-complex to induce formation of rhodium-nitrenoid complexes even using organic azides such as simple alkyl azides without strong electron-withdrawing substituents.

In this study, we succeed in developping a C–H bond amination reaction using $[Rh^{II}(TMAA)]_2$ and non-activated alkyl-azides as the catalyst and the nitrene source, respectively, and characterising the rhodium-nitrenoid intermediate as the active oxidant. The intermediate has a nitrogen atom that does not obey a octet rule. The ChemDraw structures of the rhodium complexes reported in this study are illustrated in Fig 2(b).

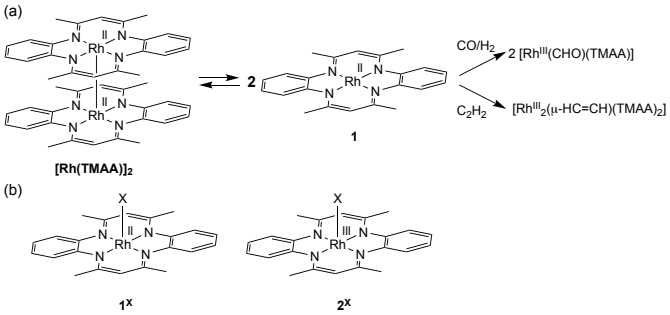

Fig. 2 The rhodium dimer complex, $[Rh^{II}(TMAA)]_2$, and reactivity of the monomer complex **1**. (b) ChemDraw structures of the rhodium(II) and rhodium(III) complexes, $\mathbf{1^X}$ and $\mathbf{2^X}$, reported in this study. X denotes monodentate ligand.

Results and discussion

C-H Amination

First, catalytic activity of $[Rh(TMAA)]_2$ was examined in intramolecular amination of trisylazide (N_3-Trs). The results are summarized in Table 1. A treatment of N_3-Trs (70 μmol) with a catalytic amount of $[Rh(TMAA)]_2$ (5 mol%) in toluene at 50 ºC for 24 h under the dark and argon atmosphere gave sultam (5,7-diisopropyl-2,3-dihydro-3,3-dimethyl-1,2-benzothiazole-1,1-dioxide) in a high yield (84%) (entry 2), where the total turnover number (TON) of the catalyst was 17. Such an amination reaction did not proceed at all in the absence of $[Rh(TMAA)]_2$ even at a higher temperature (100 °C) (entry 1). Employment of $[Rh_2(OAc)_4]$ as a typical dirhodium(II) complex instead of $[Rh(TMAA)]_2$ hardly produced the product (0.53%) (entry 7), showing that $[Rh(TMAA)]_2$ was a much better catalyst when compared with $[Rh_2(OAc)_4]$ in the C–H amination reaction of N_3-Trs. When the reaction temperature was raised to 70 ºC and 100 ºC (entries 3 and 4), the product yield increased up to 93%. This yield also was higher than that with $[Rh_2(OAc)_4]$ (entry 8). On the other hand, the product yield was lower as 79 % at a shorter reaction time (6 h) (entry 5). When the amount of trisylazide was increased from 70 μmol to 700 μmol (entry 6), TON of the catalyst reached to 653 with keeping the high product yield (93%). By these experiments, $[Rh^{II}(TMAA)]_2$ was revealed to work as a catalyst for C-H amination.

Table 1 Intramolecular Amination of Trisylazide (N_3-Trs)[a]

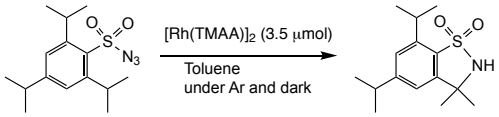

Entry	Cat. (mol %)	Temp. (ºC)	Time (h)	Sultam[b] % (μmol)	TON[c]
1	0	100	24	0	0
2	5.0	50	24	84 (59)	17
3	5.0	70	24	87 (61)	17
4	5.0	100	24	95 (67)	19
5	5.0	100	6	79 (55)	16
6[d]	0.5	100	24	93 (653)	186
7[e]	5.0	50	24	0.53 (0.37)	0.11
8[e]	5.0	100	24	16 (11)	3

[a] Reaction conditions: $[Rh(TMAA)]_2$ (3.5 μmol), trisylazide (70 μmol), in toluene (1 mL), under dark and Ar atmosphere. [b] Product yields (based on N_3-Trs) determined by ^{1}H NMR spectra. The amounts are shown in parentheses. [c] TON = (amount of product)/(amount of catalyst). [d] With 700 μmol of trisylazide. [e] $[Rh_2(OAc)_4]$ was used instead of $[Rh(TMAA)]_2$.

Table 2 Intramolecular Amination of Aliphatic Azides[a]

Entry	Cat.	Substrate	Product	%[b] (μmol)	TON[c]
1[d]	$[Rh(TMAA)]_2$	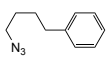	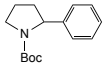	16 (7.7)	3.2
2[d]	$[Rh_2(OAc)_4]$			0 (0)	0

3[d]	[Rh(TMAA)]$_2$	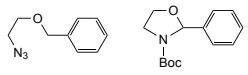	6 (4.4)	1.3
4[d]	[Rh$_2$(OAc)$_4$]		0 (0)	0

[a] Reaction conditions: Rh-catalyst (3.5 μmol), substrate (70 μmol), in toluene (1 mL) under dark and Ar atmosphere, for 24 h, at 100 ºC. [b] Product yields (based on N_3-Trs) determined by ^{1}H NMR spectra. The amounts are shown in parentheses. [c] TON = (amount of product)/(amount of catalyst). [d] $(Boc)_2O$ (70 μmol) was added as an additive.

Catalytic activity of [Rh(TMAA)]$_2$ was then examined in intramolecular amination of other organic azides (Table 2). Benzylic C–H amination of 4-phenyl-butylazide proceeded to yield 2-phenylpyrrolidine, even though the yield was lower (16%) (entry 1). Its ether derivative, benzyl-2-azidoethyl-ether, also was converted to the pyrrolidine derivative in a 6% yield (entry 3). In these reactions as well, [Rh$_2$(OAc)$_4$] did not work as the catalyst at all (entries 2 and 4), indicating that [Rh(TMAA)]$_2$ worked well when compared with [Rh$_2$(OAc)$_4$] in activation of these organic azides with no sulfinyl (-SO_2R") and carboxyl (-CO_2R") groups. In Table 3 are shown the results of intermolecular C–H amination of xanthene with organic azides without sulfonyl group. By amination of xanthene with benzyl azide, a small amount of the corresponding amine was produced (entry 1). The amination with 4-nitro-phenylazide proceeded to yield the amine (entry 3). Use of adamanthylazide resulted in formation of bixanthenylidene (9-(9*H*-xanthen-9-ylidene)-9*H*-xanthene) instead of the corresponding amine (entry 5). Neither anti-Bredt imine nor hemiaminal that arised from 2-azahomoadamant-3-ene was produced. It has been reported that 2-azahomoadamant-3-ene is generated by C-to-N migration of adamantylnitrene by photolysis of an adamantylazide adduct of a paddle-wheel dirhodium(II) complex.[18] On the other hand, these amination reactions did not proceed at all if [Rh$_2$(OAc)$_4$] was employed (entries 2 and 4). By collecting these results, [Rh(TMAA)]$_2$ was found to be applicable to a C-H amination catalyst with non-activated azides thought their yields were low. Under the reaction conditions given in Tables 1-3, no benzylamine derivative that derived from toluene was obtained.

Table 3 Intermolecular Amination of Xanthene[a]

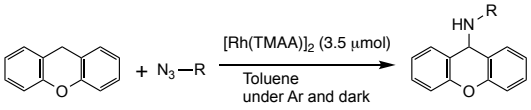

Entry	Cat.	Azide	Amine, % (μmol) [b]	TON[c]
1	[Rh(TMAA)]$_2$	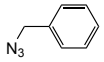	1.4 (1)	0.3
2	[Rh$_2$(OAc)$_4$]		0 (0)	0
3	[Rh(TMAA)]$_2$	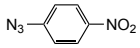	6.7 (5)	1.4
4	[Rh$_2$(OAc)$_4$]		0 (0)	0
5	[Rh(TMAA)]$_2$	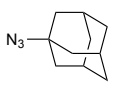	0 (0)) [d]	0

[a] Reaction conditions: Rh-catalyst (3.5 μmol), xanthene (70 μmol), in toluene (1 mL) under dark and Ar atmosphere, for 24 h, at 100 ºC. [b] Product yields (based on N_3-Trs) determined by ^{1}H NMR spectra. The amounts are shown in parentheses. [c] TON = (amount of product)/(amount of catalyst). [d] bixanthenylidene was obtained (36 %).

Mechanistic Studies

In C-H amination reactions catalysed by the paddle-wheel rhodium(II) dimers, [$Rh^{II}_2(R_1COO)_4$], a rhodium-nitrenoid intermediate, [$Rh^{II}_2(NR)(R_1COO)_4$], has been identified as the active-oxidant, where the nitrenoid complex has the dirhodium(II) triplet nitrene electronic structure (Fig. 1).[13,14] The intermediate is stabilised by π-back donation from the filled two π* orbitals in the Rh^{II}-Rh^{II} bond to the half-filled two 2p orbitals of the NR moiety.[13,14] To obtain mechanistic insights into the catalytic cycle of the present C-H amination reaction with [Rh(TMAA)]$_2$, we tried to characterise the active oxidant. Fig. 3 shows UV-vis spectral changes of [Rh(TMAA)]$_2$ in toluene by adding various amounts of ferrocenium hexafluorophosphate ($FcPF_6$) as an oxidant, where the absorption bands at 662 and 395 nm due to the dimer complex (red lined spectrum) decreased with concomitant increase of the new absorption bands at 529 and 343 nm (blue lined spectrum) with clear isosbestic points at 605, 444, and 359 nm. The spectral change completed when 2 equiv. of the oxidant was added (Fig. 3, inset). During standing the solution in the cell for 60 min, a red-brown microcrystalline powder precipitated.

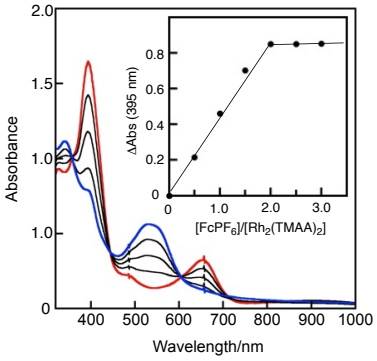

Fig. 3 UV-vis spectral changes observed in the titration of [Rh(TMAA)]$_2$ (50 μM, red) by ferrocenium hexafluorophosphate ($FcPF_6$) in toluene at 40 °C. (inset) Plot of absorbance at 395 nm against [$FcPF_6$]/[(Rh(TMAA)$_2$] in the titration experiment.

Then, we tried to isolate the sample in a preparative scale to obtain [Rh(TMAA)(CH_3CN)](PF_6) (**2**^{CH3CN}), and single crystals suitable for X-ray crystallographic analysis were obtained in a 61% yield by recrystallization of the powder sample from CH_3CN/Et_2O. Fig. 4(a) shows the crystal structure of **2**^{CH3CN}. The Rh(1) center exhibits a distorted square pyramidal structure with four nitrogen atoms of doubly deprotonated ligand $TMAA^{2-}$ at the equatorial positions and one nitrogen atom of acetonitrile at the axial position. In this structure, one carbon atom, C(1), of the ligand in a neighboring rhodium complex interacts with the Rh(1) atom (Fig. S1(a)). Oxidation

number of the rhodium centre is deduced as +III from the charge balance, which is consistent with its diamagnetic character of the oxidized complex as revealed by the ^{1}H NMR spectrum (see experimental section). In a preparative experiment using pyridine as a solvent instead of CH_3CN, [Rh(TMAA)(C_5H_5N)](PF_6), ($\mathbf{2}^{\mathbf{Py}}$), was isolated. As shown in Fig. 4(b), the overall structure of the Rh(1) centre is similar to that **of** $\mathbf{2}^{\mathbf{CH3CN}}$ except the presence of pyridine as the axial ligand instead of CH_3CN of $\mathbf{2}^{\mathbf{CH3CN}}$. As found in the crystal structure of $\mathbf{2}^{\mathbf{CH3CN}}$, $\mathbf{2}^{\mathbf{Py}}$ also exhibits intermolecular interaction with a ligand carbon atom C(1) of a neighboring complex (Fig. S1(b)). Similar intermolecular interaction between two molecules of rhodium(III) complexes of $TMAA^{2-}$ has been found in [Rh(TMAA)(CHO)] ($\mathbf{2}^{\mathbf{CHO}}$) and [Rh(TMAA)(Et)] ($\mathbf{2}^{\mathbf{Et}}$).[17] It should be noted that there is no direct rhodium–rhodium bonding interaction in the oxidized Rh(III)-complexes $\mathbf{2}^{\mathbf{X}}$ (X = CH_3CN, Py, CHO, Et). From these results, it was found that rhodium(III) monomer, $[Rh(TMAA)]^+$ (**2**), was generated by oxidizing $[Rh(TMAA)]_2$ in toluene. An aspect of UV-vis spectrum of $\mathbf{2}^{\mathbf{CH3CN}}$ in CH_3CN is very close to that finally observed one in Fig. 3, indicating that a strong absorption band around 550 nm is supportive of formation of a rhodium(III) monomer complex with $TMAA^{2-}$.

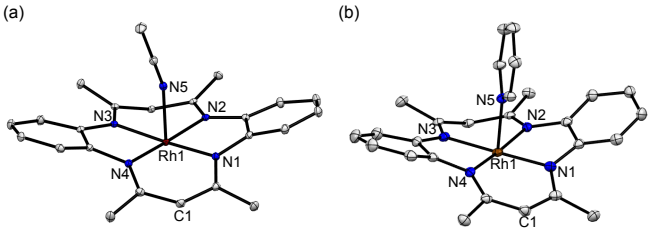

Fig. 4 Crystal structures of (a) $\mathbf{2}^{\mathbf{CH3CN}}$ and (b) $\mathbf{2}^{\mathbf{Py}}$. Hydrogen atoms, counter anions, and solvent molecules are omitted for clarity.

Then, a reaction of $[Rh(TMAA)]_2$ with an organic azide was monitored by UV-vis spectroscopy. The spectral change with N_3-Trs in toluene was complicate at room temperature, but it became simpler at lower temperature. Fig. 5(a) shows a spectral change observed upon an addition of 2 equiv of N_3-Trs to a toluene solution of $[Rh(TMAA)]_2$ at -70 ºC. As the reaction proceeded, the absorption bands at 654 and 390 nm (red line spectrum) decreased with concomitant increase of a new absorption band at 599 nm (blue line spectrum) keeping isosbestic points at 767, 682, 629, 493, and 472 nm. When the solution temperature was raised from -70 °C to -20 ºC, further spectral change was observed. As shown in Fig. 5(b), the absorption band at 599 nm observed at -70 ºC decreased with concomitant increase of a new absorption band at 545 nm. After a work up treatment, formation of the amination product, sultam, was confirmed by the ^{1}H NMR spectrum. The finally recorded spectral profile that has an absorbance at λ_{max} (545 nm) at –20 °C is close to that (529 nm) of the rhodium(III) monomer generated by the oxidation of $[Rh(TMAA)]_2$ with 2 equiv. of $FcPF_6$. If $TMAA^{2-}$-based oxidation took place in the reaction, the generated diiminobenzosemiquinone moiety would show absorption bands from 700 to 1000 nm.[19] Collectively, it was revealed that the reaction of $[Rh(TMAA)]_2$ with an organic azide caused rhodium(II)-centered oxidation to give a rhodium(III) species with dianionic TMAA ligand.

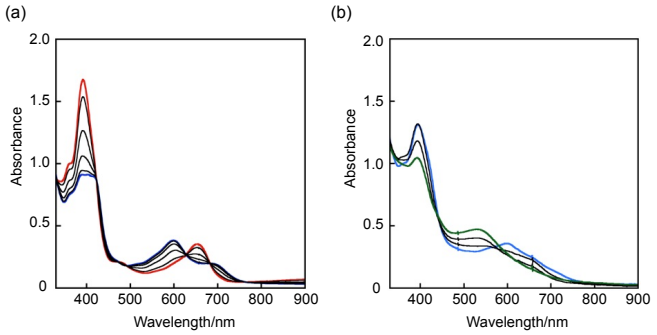

Fig. 5 (a) UV-vis spectral change observed in the reaction of $[Rh(TMAA)]_2$ (50 μM, red) with 2 equiv of N_3-Trs in toluene at -70 °C (red line to blue line). (b) Further spectral change observed when the temperature of the solution was raised from -70 °C to -20 °C (sky-blue line to green line).

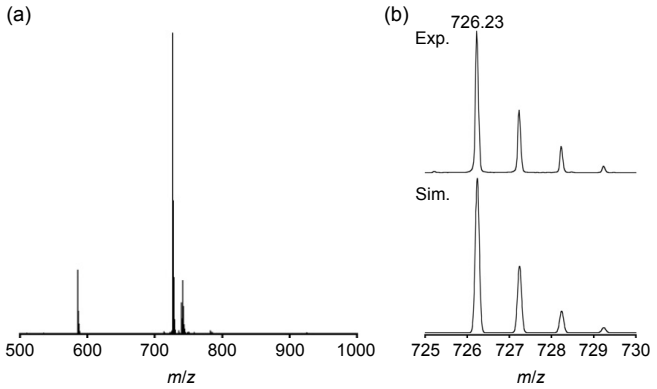

Fig. 6 (a) ESI-mass spectrum of a reaction solution of $[Rh(TMAA)]_2$ with 2 equiv of N_3-Trs in toluene at -20 °C. (b) An expanded spectrum around at m/z = 726.23 and simulated spectrum as [Rh(TMAA)(N-Trs)].

To characterise the generated species at -20 ºC, an electro-spray-ionization mass spectrum (ESI-MS) of the post reaction solution was measured. As shown in Fig. 6(a), there was a peak cluster at m/z = 726.23, the isotope distribution pattern of which was consistent with the chemical formula of the rhodium nitrenoid, [Rh(TMAA)(N-Trs)], or the sultam adduct rhodium complex, [Rh(TMAA)(sultam)] (Fig. 6(b)). In a IR spectrum of a reaction solution of $[Rh(TMAA)]_2$ and 2 equiv, of N_3-Trs at -20 ºC in toluene, no ν(N≡N) stretch band was observed around 2100 cm^{-1}, but peaks at 1179 cm^{-1} and 1378 cm^{-1} that can be attributed to the ν(S=O) stretches were observed (Fig. S2). The results of the IR measurements indicate that N_3-Trs was converted to N-Trs or sultam at -20 ºC. Then, *p*-nosylazide (N_3-Ns: N_3-SO_2-C_6H_4-*p*-NO_2) was employed as an organic azide to further characterise the generated species at -20 ºC, since it does not have a C(sp^3)-H bond and, hence, does not undergo intramolecular amination. As shown in Fig. 7(a), the ESI-mass spectrum of a reaction solution of $[Rh(TMAA)]_2$ and 2 equiv of N_3-Ns in toluene showed the presence of [Rh(TMAA)(N-Ns)] at m/z = 645.07. In the IR spectrum of the reaction solution (Fig. S3), there was no peak due to ν(N≡N) stretch of N_3-Ns. These spectral data suggest that the product obtained at –

20 °C was the rhodium-nitrenoid complex. ESI-mass spectrum of the reaction solution of $[Rh^{II}(TMTAA)]_2$ with N_3-CH_2Ph was also measured to see whether the corresponding rhodium-nitrenoid complex was formed by the reaction. As the result, a peak cluster due to the corresponding rhodium-nitrenoid species, $[Rh^{III}(TMTAA)(NCH_2Ph)]$, was observed at m/z = 550.12 (Fig. S4).

X-band electron paramagnetic resonance (EPR) spectrum of the reaction solution of $[Rh(TMAA)]_2$ with 2 equiv. of N_3-Ns exhibited a signal assignable to spin doublet species with relatively small rhombicity as for Rh(II) species (Fig. 7(b)).[20-22] The g-values (2.058, 1.994, 1.949) of the spectrum were obtained from its simulation with hyperfine coupling constant of a nitrogen atom (A = 22.4 G, 10.6 G, 11.8 G) calculated with DFT for $[Rh^{III}(N^{\bullet}\text{-Ns})(TMAA^{2-})]$ (Fig. S5). The g_{iso} value of 2.000 is close to the values obtained for organic radicals coordinating a rhodium(III) center.[23-25] As mentioned above, reactions of $[Rh(TMAA)]_2$ with $FcPF_6$ and N_3-R do not cause oxidation of phenylene diamido moieties but resulted in formation of rhodium(III) complexes. By combining the above spectroscopic results, it is suggested that the generated rhodium-nitrenoid complex is likely to have an electronic structure of a rhodium(III) nitrene radical complex, $[Rh^{III}(TMTAA)(N^{\bullet}\text{-R})]$ (R = Trs, $\mathbf{2}^{\mathbf{N\bullet Trs}}$; = Ns, $\mathbf{2}^{\mathbf{N\bullet Ns}}$), where a spin is mainly localized on the septet nitrogen atom. One-electron reduction of the azide moiety by one rhodium(II) centre resulted in formation of the complex (Scheme 1). Such electronic structure was also rationalized by DFT calculation for [Rh(N-Ns)(TMAA)] (Fig. S5). Such formation of a metal-nitrene radical complex accompanied with a one-electron oxidation of metal centre has been found in other systems, e.g. iron(III) dipyrrin complexes, cobalt(III) porphyrin complexes, nickel(II) dipyrrin, nickel bis(aminoalkyl)amine complexes.[26-34] With respect to the intermediate observed at -70 ºC, it may be a mono- or di-sulfonylazide adduct of $[Rh(TMAA)]_2$, $[Rh(TMAA)(N_3\text{-Trs})]_2$, $[Rh_2(TMAA)_2(N_3\text{-Trs})]$, or a mono-sulfonylazide adduct of **1**, $[Rh^{II}(TMTAA)(N_3\text{-Trs})]$ ($\mathbf{1}^{\mathbf{N3\text{-}Trs}}$).

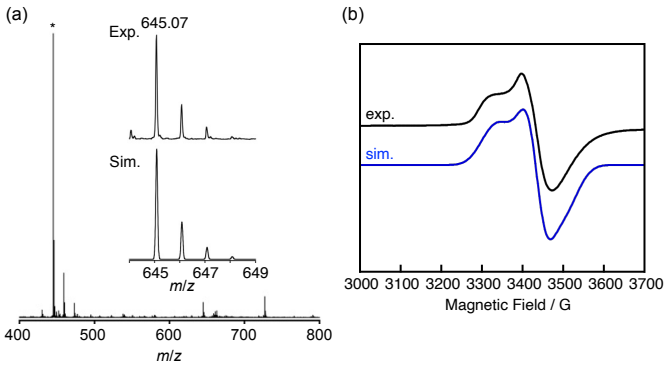

Fig. 7 (a) An ESI-mass spectrum of a reaction solution of $[Rh(TMAA)]_2$ with 2 equiv of N_3-Ns in toluene. Inset: an expanded spectrum at around m/z = 645.97 and a simulation spectrum for [Rh(N-Ns)(TMAA)]. A peak cluster marked with * corresponds to [Rh(TMAA)]. (b) An EPR spectrum (black line) of a reaction solution of $[Rh(TMAA)]_2$ with 2 equiv. of N_3-Ns in toluene measured at 110 K (Frequency: 9.576 GHz), and its simulated spectrum (blue line) with g = (2.058, 1.994, 1.949) and A = (22.4 G, 10.6 G, 11.8 G), g_{iso} = 2.000.

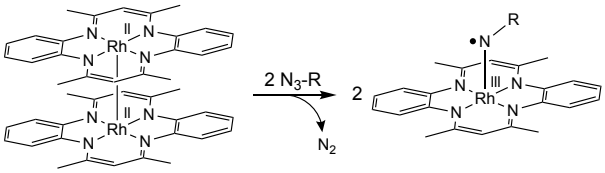

Scheme 1. Formation of Rhodium(III)-nitrenoid Complex.

To obtain insights into the electronic structure of the present rhodium(III)-nitrenoid complex $\mathbf{2}^{\mathbf{N\bullet Trs}}$ and the amination reaction mechanism, DFT calculations were performed. The spin density plots of $\mathbf{2}^{\mathbf{N\bullet Trs}}$ is shown in Fig. 8(a), where the SOMO consists of a dπ-pπ ($Rh4d_{zx}$-$N2p_x$) anti-bonding orbital (Fig. 8(b)). Thus, the spin density on the NTrs nitrogen atoms is 0.76 while that on the Rh atoms is only 0.14. The calculated spin-density distribution is consistent to the large hyperfine coupling due to the nitrogen nucleus as observed in the EPR experiment (*vide supra*). On the other hand, dσ-pσ ($Rh4d_{z2}$-$N2p_z$) anti-bonding interaction makes the LUMO (Fig. 8(c)) and, hence, another dπ-pπ ($Rh4d_{yz}$-$N2p_y$) interaction provides the filled π and π* orbitals (Fig. 8(d)). Therefore, formation of the rhodium(III) nitrene radical species involves formally an intramolecular one-electron transfer from the rhodium(II) center to the nitrene nitrogen atom. The calculated Rh^{III}–$N^{\bullet}Trs$ bond length is 1.935 Å, which is significantly longer than the Rh^{III}=N double bond in the tetrahedral $[Rh^{III}(NAd)(PhB(CH_2PPh_2)_3)]$ (1.780(2) Å, Ad = adamantly).[35] Thus, the computed result suggests that TsN–Rh^{III} bond has a single bond character. Since monomer rhodium(II) complex, **1**, that was generated by dissociation of $[Rh(TMAA)]]_2$ has been proposed to react with CO/H_2 in formation of a rhodium(III) formyl complex from $[Rh(TMAA)]]_2$ under CO/H_2 atmosphere, a reaction of **1** with N_3-Trs was taken into account for the calculations.[17] Also, there was no induction period when yields of sultam were monitored against the reaction time in the catalytic amination of N_3-Trs (Fig. S6), indicating that decomposed species of $[Rh(TMAA)]]_2$ is not involved in the catalytic cycle. The calculated SCF energy profile for formation of $\mathbf{2}^{\mathbf{N\bullet Trs}}$ and the successive intramolecular C–H amination is presented in Fig. 9. $\mathbf{2}^{\mathbf{N\bullet Trs}}$ is generated from $[Rh(TMAA)]_2$ and N_3-Trs, where N_2 elimination from the azide adduct $\mathbf{1}^{\mathbf{N3Trs}}$ proceeds with $\Delta E^{\neq}$ = 4.5 kcal/mol. The first step of the amination involves intramolecular hydrogen atom abstraction from the isopropyl group by the nitrene radical moiety to yield an intermediate $\mathbf{2}^{\mathbf{NHTrs\bullet}}$ (3.0 kcal/mol). This step requires a transition state TS1 with a barrier of 14.7 kcal/mol. Then, a subsequent radical rebound process takes place *via* a transition state TS2 with a low barrier of 3.3 kcal/mol to yield the product complex $\mathbf{1}^{\mathbf{sultam}}$. When a 1 : 1 mixture of xanthene (17.5 μmol) and dideuterated-xanthene (xanthene-d_2, 17.5 μmol) was aminated with 4-nitrophenylazide under the same conditions shown in entry 3 of Table 3, a kinetic isotope effect (KIE) of 6.5 was obtained, which is close to those observed in the amination reactions of xanthene with other metal-nitrene radical complexes of rhodium(III) and tin(II) (KIE 5.7 at 375 K and 5.6 at 375 K, respectively),[24,36] being consistent with involvement of hydrogen atom abstraction in the present case.

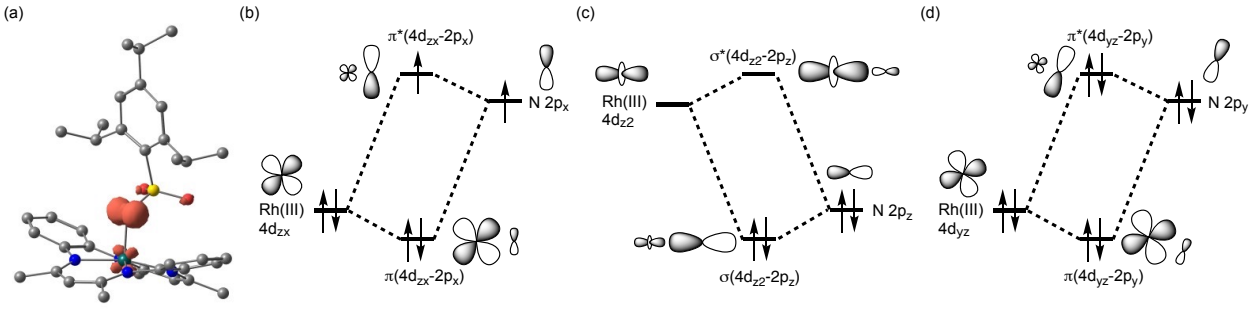

Fig. 8 (a) DFT calculated structure of $\mathbf{2}^{\mathbf{N\bullet Trs}}$ and the spin density plot: green: rhodium, blue: nitrogen, red: oxygen, yellow: sulfur, gray: carbon. (b, d) dπ-pπ interaction and (c) dσ-pσ interaction of $\mathbf{2}^{\mathbf{N\bullet Trs}}$.

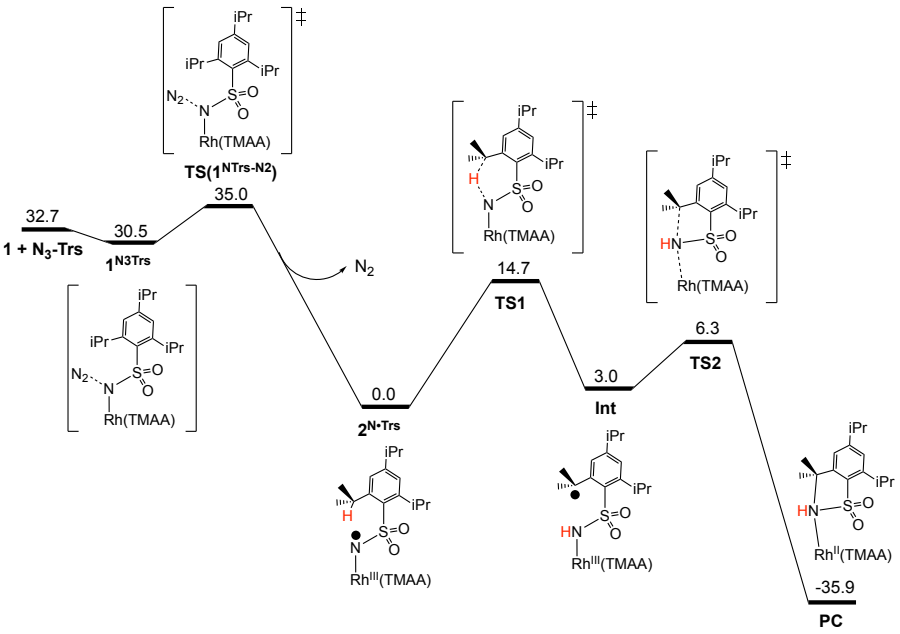

Fig. 9 A calculated reaction pathway for C-H amination of trisylazide with **1** in the doublet state at the B3LYP level. Relative electronic energies with respect to $\mathbf{2}^{\mathbf{N\bullet Trs}}$ are reported in units of kcal/mol.

Conclusions

We presented a new protocol employing a rhodium(II) dimer, $[Rh^{II}(TMAA)]_2$ as a catalyst for the C-H amination with organic azides. Various types of organic azides containing electron-rich or electron-deficient substituent were available. By a combination of spectroscopic methods and DFT calculations for the reactions of **1** with trisylazide and nosylazide, the generated rhodium imido species have been confirmed to be the rhodium(III)-nitrenoid complexes that possess a spin localizing on the nitrene nitrogen atom, $[Rh^{III}(TMAA)(N^{\bullet}\text{-Trs/Ns})]$ ($\mathbf{2}^{\mathbf{N\bullet Trs/Ns}}$). The kinetic isotope effect (KIE) for the C-H amination of xanthene with 4-nitrophenylazide and DFT calculations for C-H amination of trisylazide suggested that hydrogen atom abstraction from the aliphatic substrates with $\mathbf{2}^{\mathbf{N\bullet Trs/Ns}}$ is involved in the C-H amination reactions. Because the rhodium(III)-nitrenoid species in the present protocol is a novel active oxidant in dirhodium(II) catalyzed direct C-H amination and the reactivity can be controlled by changing substituents of the azides, the present protocol opens further development of C-H amination method of alkanes.

Experimental

Materials and methods

General. Reagents and solvents used in this study except the rhodium complex and organic azides were commercial products of the highest available purity. The solvents were stored with molecular sieve 4A under argon. The *p*-nosylazide[37], trisylazide,[38] 4-azido-1-phenylbutane,[39] benzyl-2-azidoethyl-ether,[39] 4-nitrophenylazide[40] and benzylazide[41] were synthesised by following the literature methods. The rhodium(II) dimer, $[Rh^{II}(TMAA)]_2$, was prepared by following the reported procedure.[15] All sample solutions used for spectroscopic measurements were prepared under argon in a Miwa DB0-1KP glovebox. ^{1}H NMR spectra were recorded on a JEOL ECS 400 spectrometer (400 MHz). EPR spectra were taken on a BLUKER X-band spectrometer under non-saturating microwave power conditions (1.0 mW) operating at 9.576 GHz. UV-vis spectra were recorded on a Hewlett Packard 8453 photo diode array spectrophotometer equipped with a UNISOKU thermo-stated cell

holder (USP-203). Solution IR spectra were taken on a SHIMADZU spectrometer (IRPrestige-21) equipped with a UNISOKU thermo-stated cell holder (USP-203).

[Rh^{III}(TMAA)(CH$_3$CN)](PF$_6$) (2^{CH3CN}). Acetone (0.4 mL) was added to ferrocenium hexafluorophosphate ($FcPF_6$, 0.033 mmol, 11 mg), and the resultant suspension was added dropwise to a green toluene solution (2.0 mL) of $[Rh(TMAA)]_2$ (0.0112 mmol, 10 mg). The reaction mixture turned to purple during stirring for 30 min. After 10 min, a red powder was precipitated, which was collected by filtration. The crude product was recrystallised by vapor diffusion of Et_2O into the CH_3CN solution (6 mg, 61%). ^{1}H NMR (CD_3CN, 400 MHz): δ = 7.51 ppm (d, J = 8.5 Hz, 4H), 7.41 (t, J = 8.5 Hz, 4H), 7.21 (t, J = 7.8 Hz, 4H), 6.86 (t, J = 7.8 Hz, 4H), 5.41 (s, 2 H), 4.71 (d, J = 3.7 Hz, 2H), 2.63 (s, 12H), 2.22 (s, 12H).

[Rh^{III}(TMAA)(C$_5$H$_5$N)](PF$_6$) (2^{Py}). $FcPF_6$ (11 mg, 0.033 mmol) dissolved in acetone (0.4 mL) was added dropwise to 2.0 mL of a toluene solution of $[Rh(TMAA)]_2$ (10 mg, 0.011 mmol). The reaction solution turned to purple in color during stirring for 30 min. A red powder precipitated from the mixture was collected by filtration and dried in air. The powder sample (3.0 mg) was dissolved in 30 μL of pyridine, from which red crystals of **2^{Py}** were obtained by adding Et_2O to the pyridine solution. Yield: 3.0 mg (20%). Anal. Calcd for $[Rh(TMAA)(C_5H_5N)](PF_6)\bullet 2H_2O$ ($C_{27}H_{31}F_6N_5O_2PRh$): C, 45.97; H, 4.43; N, 9.93. Found: C, 45.97; H, 4.23; N, 9.67.

Monitoring Absorption Spectral Change of [Rh(TMTAA)]$_2$. 2.0 mL of a toluene solution of the dirhodium(II) complex (50 μM, 0.1 μmol) was prepared first and the solution was transferred into a 1.0 cm path length UV-vis cuvette. The cuvette was held in a Unisoku thermostated cuvette holder set at -70 ºC. 1.0 mL of a toluene solution of trisylazide (5000 μM, 5.0 μmol) was prepared and 40 μL of the solution was added to the toluene solution in the cuvette through a septum cap by using a gas-tight syringe. The solution temperature was controlled in a UNISOK thermo-Stated cell holder (USP-203).

EPR Measurement. An EPR tube (ϕ=ca.5 mm) containing a toluene solution (0.3 mL) of $[Rh(TMAA)]_2$ (0.5 mM) was kept at -70 ºC using a dry ice-acetone bath. To the toluene solution, a toluene solution of *p*-nosylazide was added through a septum cap by using a gas-tight syringe ([$[Rh(TMAA)]_2$] : [*p*-nosylazide] = 1 : 2). After standing at -20 ºC for 1 h to generate **2$^{N\bullet Ns}$**, the color of the solution changed from green red. The solution was frozen in liquid nitrogen and the tube was put in the cavity. EPR spectrum of the solution was recorded with X-band microwave (9.576 GHz) at 110 K. Microwave power of 1.0 mW and modulation amplitude of 0.50 G were employed in the measurement. The obtained spectrum was simulated with a software SimFonia to provide EPR parameters of A_1 = 22.4 G, A_2 = 10.6 G, A_3 = 11.8 G, g_1 = 2.058, g_2 = 1.994, and g_3 = 1.949 (g_{iso} = 2.000).

Solution IR Measurement. A toluene solution (0.3 mL) of $[[Rh(TMAA)]_2$ (5 mM) was kept at -70 ºC using a dry ice-acetone bath, to which a toluene solution of an organic azide was added through a septum cap by using a gas-tight syringe ([$[Rh(TMAA)]_2$] : [azide] = 1 : 2). Then, the solution was heated to -20 ºC and put in an IR cell. Solution IR spectrum of the solution was recorded with a SHIMAZU Solution IR spectrometer (IRPrestige-21) with a Unisoku thermostated cryostat cell holder USP-203 at -20 ºC.

General Procedure of Intramolecular Amination Catalyzed by [Rh(TMTAA)]$_2$. An organic azide (70 μmol) was dissolved in toluene (200 μL), which was added to a toluene solution (800 μL) of the dirhodium(II) complex (3.5 μmol, 3.1 mg). In the case of amination of 1-azido-4-phenylbutyane and benzyl-2-azidoethyl ether, 200 μL of a toluene solution of Boc_2O (70 μmol, 15.3 mg) was added to the reaction solution. The solution was stirred at 100 °C for 24 h in the dark. All volatiles were evaporated in vacuo and the crude products were analyzed by ^{1}H NMR spectroscopy ($CDCl_3$, 400 MHz, Internal Standard; 1,1,2,2-tetrachloroethane (7.34 μL, 70 μmol)). The aminated products were identified by comparing their ^{1}H NMR chemical shifts to those of the known products (Figs. S7-S9). The catalytic experiments were performed at least twice for each entry.

General Procedure of Intermolecular Amination of Xanthene Catalyzed by [Rh(TMTAA)]$_2$. A toluene solution (200 μL) of an organic azide (70 μmol) was added to 800 μL of a toluene solution containing $[Rh(TMAA)]_2$ (3.5 μmol, 3.1 mg) and xanthene (70 μmol, 12.4 mg). The mixture was stirred at 100 °C for 24 h in the dark. All volatiles were evaporated in vacuo and the crude products were analysed by ^{1}H NMR spectroscopy ($CDCl_3$, 400 MHz, Internal Standard; 1,1,2,2-tetrachloroethane (7.34 μL, 70 μmol) (Figs. S10-S11).

Kinetic Isotope Effect (KIE) Measurement. A toluene solution (200 μL) of 4-nitrophenylazide (70 μmol) was added to a toluene solution (800 μL) containing $[Rh(TMAA)]_2$ (3.50 μmol, 3.12 mg), xanthene (35 μmol, 6.12 mg), and xanthene-d_2 (35 μmol, 6.70 mg). The mixture was stirred at 100 °C for 24 h. All volatiles were evaporated in vacuo and the crude products were analysed by ^{1}H NMR spectroscopy ($CDCl_3$, 400 MHz, Internal Standard; 1,1,2,2-tetrachloroethane (7.34 μL, 70 μmol) (Fig. S12). KIE was estimated as a ratio of aminated xanthene : aminated xanthene-d_2.

X-ray Crystallography. Single crystals of **2^{CH3CN}** suitable for X-ray crystallographic analysis were obtained by slow diffusion of diethyl ether into the acetonitrile solution. Single crystals of **2^{py}** suitable for X-ray crystallographic analysis were obtained by vapor diffusion of diethyl ether into the mixed solution of dimethylacetamide and pyridine. Each single crystal was mounted on a loop with a mineral oil. Data from X-ray diffraction were collected at −158 °C by a Rigaku R-AXIS RAPID diffractometer using filtered Mo-Kα radiation (λ = 0.71075 Å). The structures were solved by SHELXT[42] and expanded using Fourier techniques. The non-hydrogen atoms were refined anisotropically by full-matrix least squares on F^2. The hydrogen atoms were attached at idealized positions on carbon atoms and were not refined. All calculations were performed using the program Olex2 crystallographic software packages.[43] There is no high-level alert in the check cif file to the cif and fcf files (htpps://checkcif.iucr.org). All structures in the final stage of refinement showed no movement in atom position. The crystallographic data listed in Table S1. CCDC 2240612 and 2240613 contain the supplementary crystallographic data (CIF files) for **2^{CH3CN}** and **2^{py}**, reported in this paper respectively.

Computational Methodology. All optimized structures were obtained using B3LYP functional[44-46] as implemented in the Gaussian 16 program packages.[47] We employed the SDD basis sets[48] for the Rh atom, and the D95** basis sets[49] for the other atoms, respectively. In the present calculation, the unrestricted method was used to obtain optimized structures in the doublet state. Using the vibrational

frequency analysis, we confirmed that the obtained local minima and transition state have none and one imaginary frequency, respectively.

Conflicts of interest

There are no conflicts to declare.

Acknowledgements

This work was supported by KAKENHI (Grant-in-Aid) for Scientific Research (No. 23K04767).

References

1 J. Du Bois, *Org. Process Res. Dev.*, 2011, **15**, 758.
2 F. Collet, C. Lescot and P. Dauban, *Chem. Soc. Rev*., 2011, **40**, 1926.
3 J. L. Roizen, M. E. Harvey and J. Du Bois, *Acc. Chem. Res*., 2012, **45**, 911.
4 T. A. Ramirez, B. Zhao and Y. Shi, *Chem. Soc. Rev.*, 2012, **41**, 931.
5 J. L. Jeffrey and R. Sarpong, *Chem. Sci*., 2013, **4**, 4092.
6 M.-L. Louillat and F. W. Patureau, *Chem. Soc. Rev*., 2014, **43**, 901.
7 K. Shin, H. Kim and S. Chang, *Acc. Chem. Res*., 2015, **48**, 1040.
8 F. Wang, S. Yu and X. Li, *Chem. Soc. Rev.*, 2016, **45**, 6462.
9 J. Jiao, K. Murakami and K. Itami, *ACS Catal*., 2016, **6**, 610.
10 Y. Park, Y. Kim and S. Chang, *Chem. Rev*., 2017, **117**, 9247.
11 C. Ma, P. Fang and T.-S. Mei, *ACS Catal*., 2018, **8**, 7179.
12 A. Varela-Álvarez, T. Yang, H. Jennings, K. P. Korneck, S. N. Macmillan, K. M. Lancaster, J. B. C. Mack, J. D. Bois, J. F. Berry and D. G. Musaev, *J. Am. Chem. Soc*., 2016, **138**, 2327.
13 A. Das, Y.-S. Chen, J. H. Reibenspies and D. C. Powers, *J. Am. Chem. Soc*., 2019, **141**, 16232.
14 A. Das, C.-H. Wang, G. P. Van Trieste III, C.-J. Sun, Y.-S. Chen, J. H. Reibenspies and D. C. Powers, *J. Am. Chem. Soc*., 2020, **142**, 19862.
15 G. H. Imler, M. J. Zdilla and B. B. Wayland, *Inorg. Chem.*, 2013, **52**, 11509.
16 S. J. Van Voorhees and B. B. Wayland, *Organometallics*, 1987, **6**, 204.
17 G. H. Imler, M. J. Zdilla and B. B. Wayland, *J. Am. Chem. Soc.*, 2014, **136**, 5856.
18 A.Das, Y.-S. Chen, J. H. Reibenspies and D. C. Powers, *J. Am. Chem. Soc.*, 2019, **141**, 16232.
19 D. Fujita, A Kaga, H. Sugimoto, Y. Morimoto and S. Itoh, *Bull. Chem. Soc. Jpn*., 2020, **93**, 279.
20 B. B. Wayland, A. E. Sherry and A. G. Bunn, *J. Am. Chem. Soc.*, 1993, **115**, 7675.
21 D. W. Shaffer, S. A. Ryken, R. A. Zarkesh and A. F. Heyduk, *Inorg. Chem.,* 2011, **50**, 13.
22 A. Bakac and L. M. Thomas, *Inorg. Chem.* 1996, **20**, 5880.
23 P. Saha, A. Saha Roy, T. Weyhermüller and P. Ghosh, *Chem. Commun.*, 2014, **50**, 13073.
24 D. Fujita, H. Sugimoto, Y. Shiota, Y. Morimoto, K. Yoshizawa and S. Itoh, *Chem. Commun.*, 2017**, 53**, 4849.
25 D. Fujita, H. Sugimoto, Y. Morimoto and S. Itoh, *Inorg. Chem.*, 2018, **57**, 9738.
26 A. I. O. Suarez, V. Lyaskovskyy, J. N. H. Reek, J. I. van der Vlugt and B. de Bruin, *Angew. Chem. Int. Ed*., 2013, **52**, 12510.
27 V. Lyaskovskyy, A. I. Suarez, H. Lu, H. Jiang, X. P. Zhang and B. de Bruin, *J. Am. Chem. Soc*., 2011, **133**, 12264.
28 M. Goswami, V. Lyaskovskyy, S. R. Domingos, W. J. Buma, S. Woutersen, O. Troeppner, I. Ivanović-Burmazović, H. Lu, X. Cui, X. P. Zhang, E. J. Reijerse, S. DeBeer, M. M. van Schooneveld, F. F. Pfaff, K. Ray and B. de Bruin, *J. Am. Chem. Soc*., 2015, **137**, 5468.
29 Y. Dong, R. M. Clarke, G. J. Porter and T. A. Betley, *J. Am. Chem. Soc*., 2020, **142**, 10996.
30 Y. Dong, C. J. Lund, G. J. Porter, R. M. Clarke, S.-L. Zheng, T. R. Cundari and T. A. Betley, *J. Am. Chem. Soc*., 2021, **143**, 817.
31 S. Kundu, E. Miceli, E. Farquhar, F. F. Pfaff, U. Kuhlmann, P. Hildebrandt, B. Braun, C. Greco and K. Ray, *J. Am. Chem. Soc.*, 2012, **134**, 14710.
32 M. J. T. Wilding, D. A. Iovan, A. T. Wrobel, J. T. Lukens, S. N. MacMillan, K. M. Lancaster and T. A. Betley, *J. Am. Chem. Soc*., 2017, **139**, 14757.
33 L. Nurdin, D. M. Spasyuk, W. E. Piers and L. Maron, *Inorg. Chem*., 2017, **56**, 4157.
34 Y. Dong, J. T. Lukens, R. M. Clarke, S.-L. Zheng, K. M. Lancaster and T. A. Betley, *Chem. Sci*., 2020, **11**, 1260.
35 A. M. Geer, C. Tejel, J. A. López and M. A. Ciriano, *Angew. Chem. Int. Ed*., 2014, **53**, 5614.
36 H. Sugimoto, M. Yano, K. Sato, M. Miyanishi, K. Sugisaki, Y. Shiota, A. Kaga, K. Yoshizawa and S. Itoh, *Inorg. Chem.* 2021, **60**, 18603.
37 S. Diethelm, C. S. Schindler and E. A. Carreira, *Chem. Eur. J*., 2014, **20**, 6071.
38 J. V. Ruppel, R. M. Kamble and X. P. Zhang, *Org. Lett*., 2007, **9**, 4889.
39 E. T. Hennessy and T. A. Betley, *Science*, 2013, **340**, 591.
40 V. Babin, A. Sallustrau, O. Loreau, F. Caillé, A. Goudet, H. Cahuzac, A. Del Vecchio, F. Taran and D. Audisio, *Chem. Commun*., 2021, **57**, 6680.
41 S. G. Alvarez and M. T. Alvarez, *Synthesis*, 1997, **4**, 413.
42 G. Sheldrick, *Acta Cryst. Sec. A*, 2015, **71**, 3.
43 O. V. Dolomanov, L. J. Bourhis, R. J. Gildea, J. A. K. Howard and H. Puschmann, *J. Appl. Cryst*., 2009, **42**, 339.
44 A. D. Becke, *Phys. Rev. A*, 1988, **38**, 3098.
45 C. Lee, W. Yang and R. G. Parr, *Phys. Rev. B*, 1988, **37**, 785.
46 A. D. Becke, *J. Chem. Phys.*, 1993, **98**, 5648.
47 M. J. Frisch, G. W. Trucks, H. B. Schlegel, G. E. Scuseria, M. A. Robb, J. R. Cheeseman, G. Scalmani, V. Barone, G. A. Petersson, H. Nakatsuji, X. Li, M. Caricato, A. V. Marenich, J. Bloino, B. G. Janesko, R. Gomperts, B. Mennucci, H. P. Hratchian, J. V. Ortiz, A. F. Izmaylov, J. L. Sonnenberg, D. Williams-Young, F. Ding, F. Lipparini, F. Egidi, J. Goings, B. Peng, A. Petrone, T. Henderson, D. Ranasinghe, V. G. Zakrzewski, J. Gao, N. Rega, G. Zheng, W. Liang, M. Hada, M. Ehara, K. Toyota, R. Fukuda, J. Hasegawa, M. Ishida, T. Nakajima, Y. Honda, O. Kitao, H. Nakai, T. Vreven, K. Throssell, J. A. Jr. Montgomery, J. E. Peralta, F. Ogliaro, M. J. Bearpark, J. J. Heyd, E. N. Brothers, K. N. Kudin, V. N. Staroverov, T. A. Keith, R. Kobayashi, J. Normand, K. Raghavachari, A. P. Rendell, J. C. Burant, S. S. Iyengar, J. Tomasi, M. Cossi, J. M. Millam, M. Klene, C. Adamo, R. Cammi, J. W. Ochterski, R. L. Martin, K. Morokuma, O. Farkas, J. B. Foresman and D. J. Fox, Gaussian 16, Revision A. 03; Gaussian, Inc.: Wallingford ,CT, 2016.
48 D. Andrae, U. Haeussermann, M. Dolg, H. Stoll and H. Preuss, *Theor. Chem. Acc.*, 1990, **77**, 123.
49 T. H. Jr. Dunning and P. J. Hay, in *Modern Theoretical Chemistry*, Ed. Schaefer, H. F. III, Vol. 3 (Plenum, New York, 1977) 1-28.

